Available online at www.sciencedirect.com
ScienceDirect
Trans. Nonferrous Met. Soc. China 33(2023) 1644−1654
Transactions of Nonferrous Metals Society of China
www.tnmsc.cn

Effects of B element on microstructure and mechanical properties of B_4C_p/Al composites fabricated by ultrasound assisted casting method

Mi CHEN[1], Zhi-wei LIU[1], Yu-dong JIA[2], Shen-wei YU[3], Yuan HE[3], Bo-han ZHENG[2]

1. State Key Laboratory for Mechanical Behavior of Materials, School of Materials Science and Engineering, Xi'an Jiaotong University, Xi'an 710049, China;
2. Northwest Institute for Non-ferrous Metal Research, Xi'an 710016, China;
3. CSSC No.12 Research Institute, Xingping 713102, China

Received 13 January 2022; accepted 27 April 2022

Abstract: Ultrasound assisted casting method was applied to preparing B_4C_p/Al composites with the addition of B element by adding KBF_4 into Al−B_4C−K_2TiF_6 system. The effects of B element addition on the microstructure and mechanical properties as well as the reaction mechanism at the interface of composites were investigated. Experimental results showed that B element addition altered the B_4C_p/Al interface, induced more small-sized TiB_2 particles to distribute within the matrix. Therefore, cavitation and acoustic flow effects of the melt were intensified, which led to the breaking of B_4C clusters and finally led to the homogeneous microstructure and better mechanical properties of the composites.

Key words: B element; B_4C_p/Al composite; microstructure; mechanical properties; interface reaction; ultrasound; casting method

1 Introduction

B_4C possesses low density, high elastic modulus, good chemical stability and high abundance of B^{10} isotope, thereby B_4C_p/Al composites have been attracting much more attention in various structural applications especially in nuclear industries [1−3]. Among various fabrication methods, casting is considered to be the most cost-effective approach for large-scale production of Al matrix composites (AMCs). Direct addition of B_4C into molten Al melts, however, is rather challenging due to the poor wettability between Al and B_4C [4]. In order to overcome the above problem, Ti or Zr containing salts (K_2TiF_6 or K_2ZrF_6) are usually used to promote the incorporation of B_4C particles into molten Al (alloys), since TiB_2 (or ZrB_2) layer can be in situ formed on B_4C surface via an interface reaction of [Ti] (Zr) + [B] (from B_4C)→TiB_2 (ZrB_2), which can effectively improve the wettability between B_4C and liquid Al. Al−B_4C−K_2TiF_6 (K_2ZrF_6) system has been widely used to fabricate B_4C_p/Al composites through conventional mechanical stirring casting method [5−7].

It is well known that an ultrasound assisted casting (UAC) method has been widely used in the fabrication of in-situ or ex-situ particle reinforced AMCs, since ultrasound in molten Al can give rise to some unique effects such as acoustic cavitation as well as acoustic streaming and these effects can significantly promote the formation of in-situ formed particles, improve the particle dispersity in the Al matrix and further increase the mechanical properties of AMCs [8,9]. Recently, the UAC method has been used in our research to fabricate

Corresponding author: Zhi-wei LIU, Tel: +86-18066543603, E-mail: liuzhiwei@xjtu.edu.cn
DOI: 10.1016/S1003-6326(23)66210-7

B_4C_p/Al composites using Al(liquid)−B_4C−K_2TiF_6 system [10]. It was found that ultrasound could lead to the rapid formation of a homogeneous and compact TiB_2 layer on B_4C surface as well as improve the distribution of B_4C particles in the matrix. Accordingly, the mechanical properties of composites were effectively increased [10]. It should be noted that previous research clearly showed that the Ti addition could influence the interface reaction between Al and B_4C and further influence the microstructure as well as the mechanical properties of composites [11]. Thereby, it can be inferred that the B content in molten Al should also affect the interface reaction, the microstructure, as well as the mechanical properties of composites. So far, previous research focused on the effects of Ti and Zr elements on the interface reactions, whereas the research about the production of B_4C_p/Al composites using Al(liquid)−B_4C−K_2TiF_6 system with the addition of B element via UAC method has never been reported.

In this research, we proposed a novel approach to prepare the B_4C_p/Al composites with Al(liquid)−B_4C−K_2TiF_6 system by adding different contents of KBF_4 which provided B element via UAC method. The reaction mechanism of Al(liquid)−B_4C−K_2TiF_6−KBF_4 system was studied, and the effects of B element addition on the microstructure and mechanical properties of B_4C_p/Al composites were also investigated. A new approach was proposed to optimize the interface reactions and provide some guidance for the manufacture of B_4C_p/Al composites.

2 Experimental

2.1 Preparation of B_4C_p/Al composites

Commercially pure Al (99.7% purity) and B_4C particles (99.9% purity) with an average size of 10 μm were used as the matrix and reinforcement, respectively. The addition amount of B_4C was 10 wt.% and K_2TiF_6 (99.8% purity) with the Ti/B_4C mass ratio of 0.13 was used to improve the wettability. Firstly, the B_4C particles were blended with K_2TiF_6 and preheated at 200 ℃ for 30 min. Then, the Al ingot was melted in a graphite crucible in an electrical resistance furnace. When the temperature of pure Al melt reached and remained stable at 800 ℃, the preheated mixture of B_4C and K_2TiF_6 was added into the melt. In the meantime, high-intensity ultrasound (SONICS, USA) was introduced into the melt through a Nb alloy probe with a diameter of 2.54 cm. The power of the ultrasonic generator was 1.6 kW and the frequency was 20 kHz. After a 5 min ultrasonic treatment, the melt was poured into a steel mold to form an ingot. This sample was referred to as Sample 1. Under the same fabricating condition, two groups of KBF_4 (99.8% purity) added samples were produced, the addition amounts of KBF_4 followed the KBF_4/K_2TiF_6 molar ratios of 1 and 2, and the two samples were referred to as Sample 2 and Sample 3, respectively. The compositions of the samples are summarized in Table 1.

Table 1 Composition of samples

Sample No.	B_4C content/ wt.%	K_2TiF_6 content (Ti/B_4C mass ratio)	KBF_4 content (KBF_4/K_2TiF_6 molar ratio)
1	10	0.13	−
2	10	0.13	1
3	10	0.13	2

2.2 Sample characterization

The phase in the three samples was identified by X-ray diffraction (XRD, Bruker, D8 Advance) using Cu K_α radiation at 40 kV and 40 mA and a scan rate of 0.2 and 0.033 (°)/s, respectively. The interface products between B_4C and Al in Sample 1 were analyzed using transmission electron microscope (TEM, FEI Talos F200X), by which the high angle annular dark-field (HAADF) image, the bright-field (BF) image, the energy dispersive spectroscopy (EDS) data and the selected area electron diffraction (SAED) patterns of interface products were obtained. The microstructure of samples was examined by scanning electron microscope (SEM, s4800) equipped with EDS and field emission scanning electron microscope (FESEM MAIA3 LMH). In addition, samples were deeply etched with 2.5 vol.% HF for 10 min with the aim of revealing the three-dimensional (3D) morphology of interface.

2.3 Mechanical properties tests

The hardness (Brinell HBW, ball diameter 5 mm) of each sample was obtained by using a Brinell tester (HB−300, Huayin, Yantai, China)

under a load of 2452 N for 30 s. Six individual measurements with a 4 mm interval were carried out to evaluate the microstructural homogeneity and further obtain the average hardness values of the samples. Flat tensile samples with the gauge length of 20 mm, width of 4 mm and thickness of 3.5 mm were obtained from each sample by using a wire-electrode machine. The tensile tests were performed at room temperature using a tensile machine (CMT5305, MTS, USA) with a constant cross-head speed of 0.5 mm/min. Four individual measurements were carried out for each sample to obtain the average values of ultimate tensile strength (UTS), yield strength (YS) and elongation (EL), and based on the four measurements, the tensile properties stability of the three samples could also be evaluated.

3 Results

3.1 Phase and microstructure

Figure 1 illustrates the XRD patterns of the samples. It can be observed that, in addition to Al and B_4C, TiB_2 and Al_3BC peaks were detected in the three samples, indicating that an interfacial reaction between B_4C and liquid Al containing Ti (B) took place and the related reaction products (Al_3BC, TiB_2 and AlB_2) were generated [11,12]. It should be noted that TiB_2 and AlB_2 were hardly to be distinguished via XRD test since the lattice structure of AlB_2 was very close to that of TiB_2. Figure 2(a) illustrates a typical HAADF image of B_4C_p/Al interface in Sample 1, in which two different parts can be seen: a bright layer close to Al and a dark layer near B_4C. The EDS mapping results showed that the bright layer was concentrated with Ti and contained a small amount of B, and the corresponding SAED pattern confirmed that the bright layer was TiB_2. Apart from the TiB_2 layer, a dark sublayer close to B_4C particle can also be found. The EDS mapping results indicated that the dark sublayer was enriched with Al and contained trace amount of C. The SAED pattern in Area II confirmed that the irregular layer directly contacted to B_4C was Al_3BC.

Figure 3 shows the microstructure of the three samples with different B contents. In Sample 1, it was found that some B_4C particle clusters existed in the matrix (Fig. 3(a)). At higher magnification, an

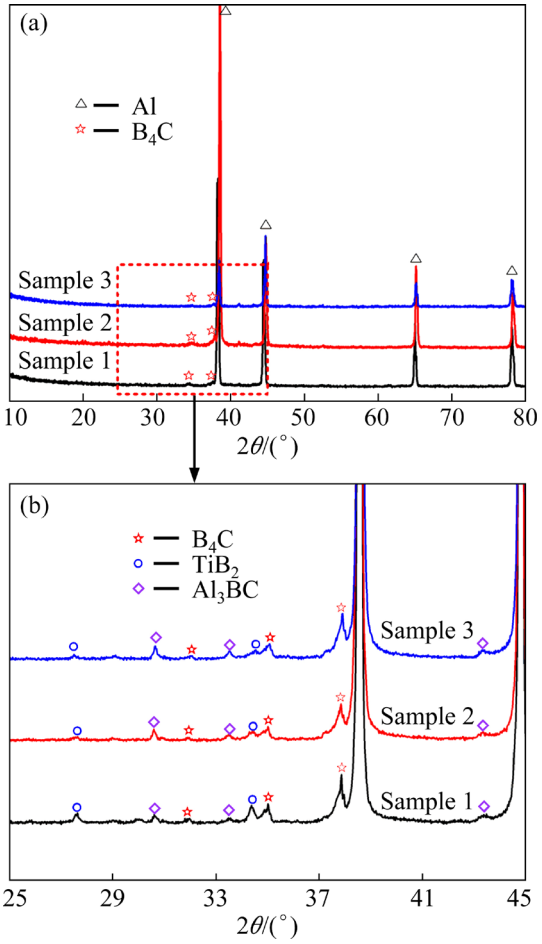

Fig. 1 XRD patterns of three samples

obvious reaction layer was observed on B_4C surface, and the related EDS mapping analyses proved that an in-situ formed TiB_2 layer was located at the interface (Fig. 3(b)). In Sample 2, the distribution of B_4C particles became more uniform (Fig. 3(c)) compared with Sample 1 and a small amount of AlB_2 particles which possessed a blocky shape with several micrometers in size, were found in the matrix (Fig. 3(d)). The corresponding EDS mapping analyses showed that the amount of TiB_2 particles on B_4C surface became less and some of which existed in the matrix. In Sample 3, it was clear that B_4C particles were distributed uniformly in the matrix and the microstructure of which was the most homogeneous (Fig. 3(f)) among the three samples. More AlB_2 particles were found in the matrix and some B_4C particles were covered by a thick Al_3BC layer in Sample 3 (Fig. 3(g)). In addition, the related EDS results combined with microstructural analyses showed that the dispersion of Ti element was improved and the amount of Ti element on B_4C surface was rather low, indicating

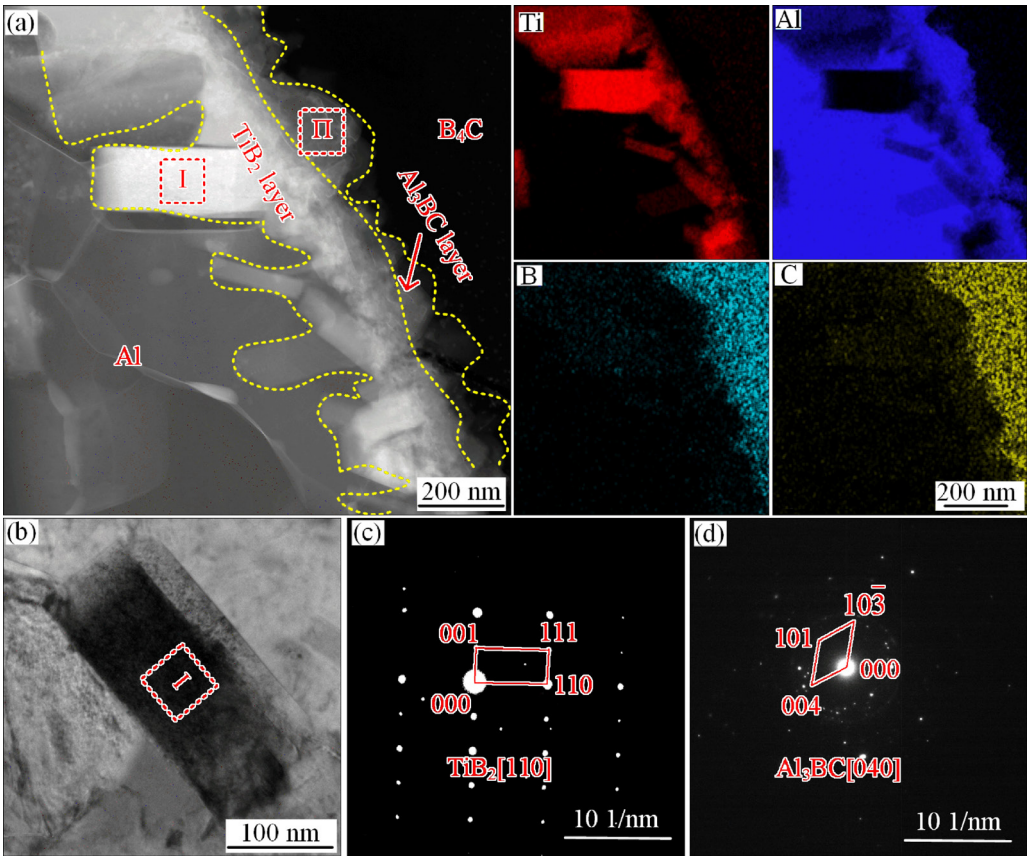

Fig. 2 HAADF image of Sample 1 (a), BF image of TiB_2 particles (b) and SAED patterns from Areas I (c) and Π (d)

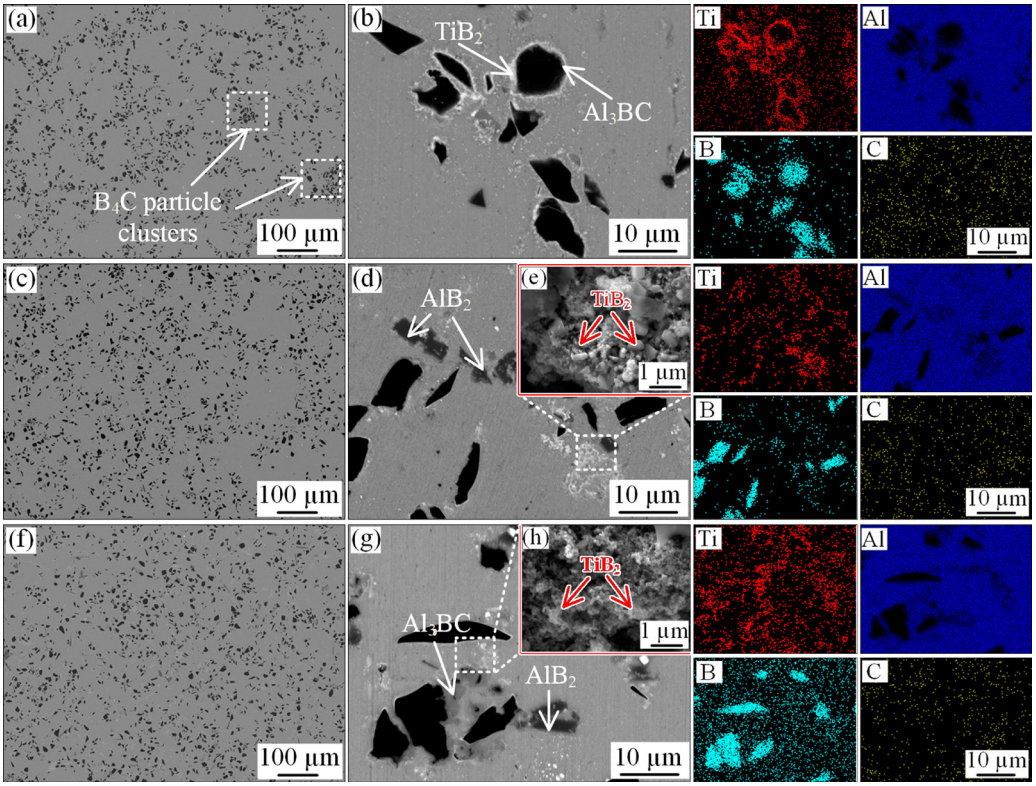

Fig. 3 SEM images and corresponding EDS analyses of B_4C_p/Al composites: (a, b) Sample 1; (c−e) Sample 2; (f−h) Sample 3

that more small-sized TiB_2 particles were distributed in the matrix. The above findings clearly indicated that adding KBF_4 into Al(liquid)−B_4C−K_2TiF_6, on the one hand, was able to enhance the homogeneity of B_4C particles in the matrix, on the other hand, could promote more small-sized TiB_2 particles to distribute in the matrix from B_4C surface.

Figure 4 showed more details of TiB_2 particles obtained by FESEM in the three samples after they were deeply etched. In sample 1, most of the TiB_2 particles distributed on the B_4C surface and the TiB_2 particles presented in the matrix were rather limited. The presence of TiB_2 can be observed on the surface of most of the B_4C particles, and only a small portion of the B_4C particles were directly exposed to the matrix (as marked by arrows in Fig. 4(a)). At higher magnification, it was clear that the B_4C particles were surrounded by a contact layer which was mainly composed of abundant hexagonal TiB_2 particles and the EDS result in Fig. 4(d) proved that the hexagonal block on B_4C surface was TiB_2. In Sample 2, more B_4C particles were directly exposed to the matrix compared with Sample 1 (as marked by arrows in Fig. 4(e)) and some TiB_2 aggregates were observed in the matrix. At higher magnification, it can be found that the TiB_2 particles mainly exhibited irregular shape and only a small number of hexagonal TiB_2 could be observed, which may be ascribed to the incomplete growth of TiB_2 particles caused by the short reaction time. As to Sample 3, almost all B_4C particles were exposed to the matrix (as marked by arrows in Fig. 4(i)) and details of the TiB_2 particles presented in the matrix were displayed in Fig. 4(j) and Fig. 4(k). It was clear that nearly all of the TiB_2 particles presented irregular shape and hexagonal TiB_2 particles were rarely found, which indicated that more TiB_2 particles were formed by the reaction between K_2TiF_6 and KBF_4.

3.2 Interfacial characteristics of B_4C in samples

As mentioned above, the B_4C_p/Al interface features had a close relationship with B content. To further reveal the interface evolution of the three samples, FESEM test was conducted on the three deeply etched samples and the results are shown in Fig. 5. In Sample 1, a thick and continuous TiB_2 layer was found on B_4C surface (Fig. 5(a)). After deeply etching treatment, it was found that a continuous and compact layer composed of TiB_2 particles exhibiting a faceted morphology with a sub-micro size was formed on B_4C surface (Fig. 5(b) and Fig. 5(c)), and the similar phenomenon has also been reported by LAI et al [13]. For Sample 2, a TiB_2 layer on B_4C surface was still presented with thinner thickness and smaller size. As to Sample 3, a small portion of B_4C surface was eroded by liquid

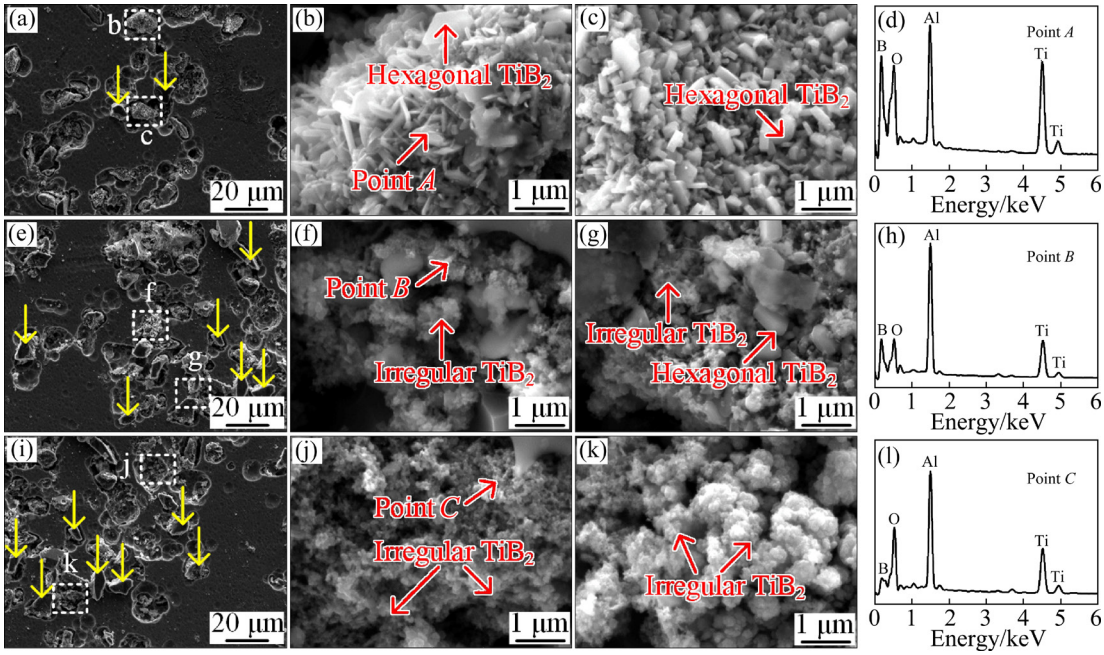

Fig. 4 FESEM images and corresponding EDS analyses of deeply etched samples: (a−d) Sample 1; (e−h) Sample 2; (i−l) Sample 3

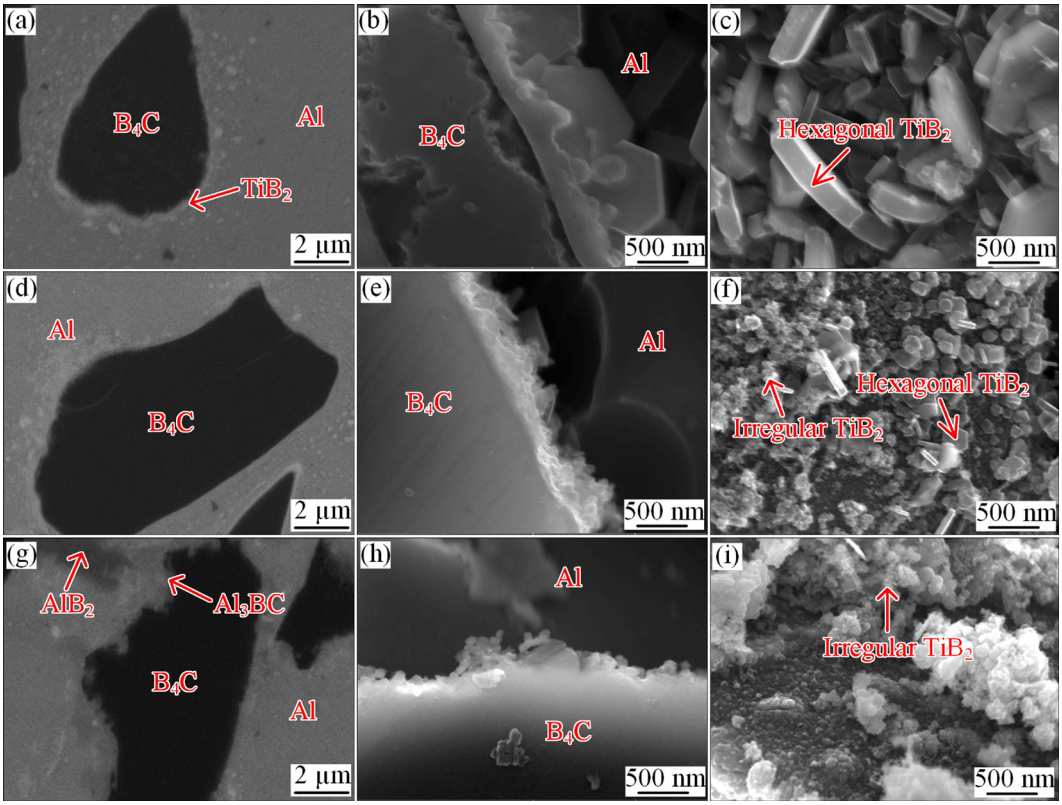

Fig. 5 FESEM images and related interfacial analyses of deeply etched samples: (a−c) Sample 1; (d−f) Sample 2; (g−i) Sample 3

Al and an obvious Al_3BC layer was found on B_4C surface (Fig. 5(g)). Furthermore, it could be found that the TiB_2 layer was composed of nano-sized TiB_2 particles with irregular shape (Fig. 5(h) and Fig. 5(i)). The above results further proved that the addition of KBF_4 could alter the B_4C_p/Al interface.

3.3 Mechanical properties of B_4C_p/Al composites

The Brinell hardness results of the samples are shown in Fig. 6. Figure 6(a) shows the Brinell hardness of six points in the three samples and Fig. 6(b) displays the average Brinell hardness values of the three samples. In Sample 1, the values of hardness ranged from 26.1 to 31.8, while in Sample 2 and Sample 3, the values of hardness ranged from 31.9 to 34.5 and 33.8 to 36.6, respectively. It was obvious that the hardness values of Sample 2 and Sample 3 fluctuated within smaller ranges in comparison with Sample 1, which suggested that the microstructures of Sample 2 and Sample 3 were more homogeneous than that of Sample 1. Moreover, the average values of hardness increased from 28.2 to 33.2 and further increased to 35.8 with increasing B content.

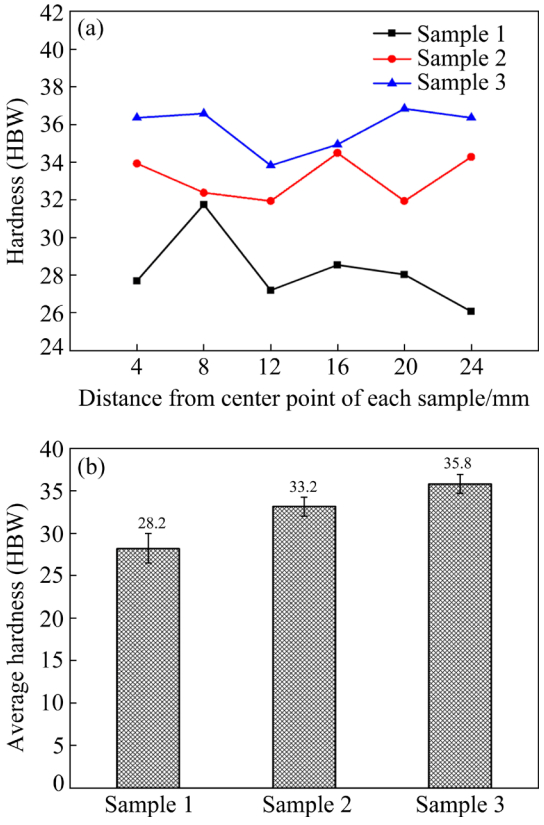

Fig. 6 Brinell hardness of six points in three samples (a) and average Brinell hardness values of three samples (b)

The tensile test results of the three samples are presented in Fig. 7. The typical tensile curves and the average values of YS, UTS and El of samples are shown in Fig. 7(a) and Fig. 7(b), respectively. The average values of YS, UTS and El of the samples were 62.0 MPa, 98.5 MPa, 12.3%, 59.3 MPa, 96.8 MPa, 17.3% and 62.5 MPa, 108.3 MPa, 17.8%, respectively. It was clear that both the YS and the UTS of Sample 2 were slightly decreased while the El was enhanced significantly (improved by 40%) in comparison with Sample 1. As to Sample 3, both the UTS (improved by 10%) and ductility (improved by 45%) were enhanced with the addition of KBF_4. In order to evaluate the tensile properties stability of the samples, the YS, UTS as well as El of four individual specimens for each sample are summarized and the corresponding results are displayed in Fig. 7(c). The YS, UTS and El of Sample 1 ranged from 59 to 67 MPa, 95 to 105 MPa, 10.2% to 16.8% while the YS, UTS and El of Sample 2 ranged from 58 to 61 MPa, 93 to 100 MPa, 16.0% to 20.0%. As to Sample 3, the YS, UTS and El fluctuated within small ranges (62 to 65 MPa, 107 to 111 MPa, 17.0% to 18.2%), which indicated that Sample 3 possessed the best stability among the three samples due to its most homogeneous microstructure.

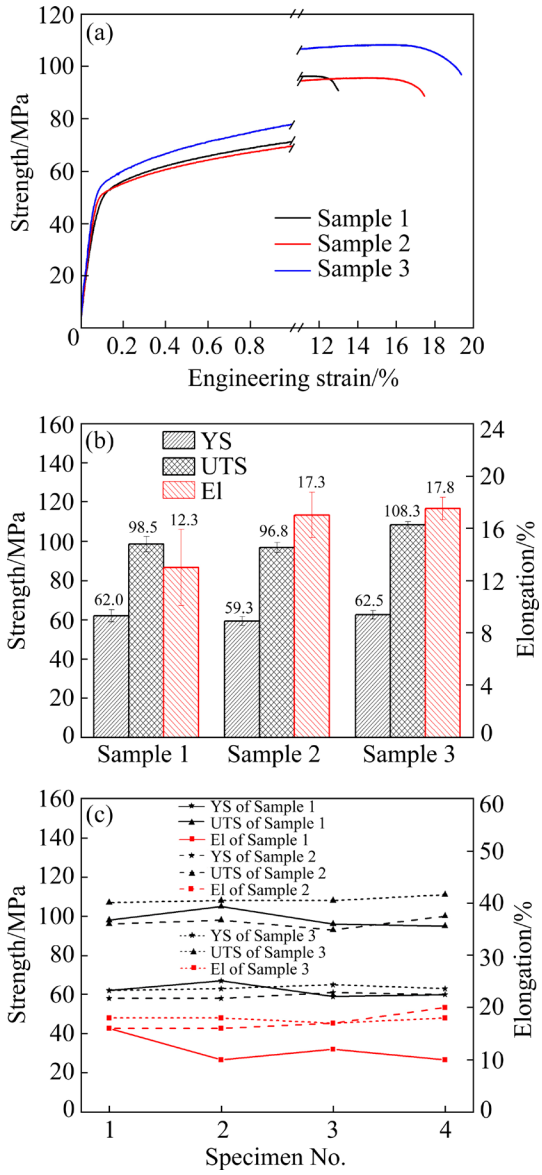

Fig. 7 Tensile test results of B_4C_p/Al composites: (a) Tensile curves; (b) Mechanical properties; (c) YS, UTS and El of four specimens of three samples

3.4 Tensile fracture surface

The morphologies showing tensile fracture surfaces of the three samples are displayed in Fig. 8. The dimples in Sample 2 and Sample 3 were larger than those in Sample 1, suggesting that Sample 2 and Sample 3 exhibited better ductility due to the more uniform microstructure compared with Sample 1. Furthermore, an intact TiB_2 layer could be observed on B_4C surface and micropores were rarely found at the B_4C_p/Al interface in Sample 1 (Fig. 8(b)). As to Sample 2 and Sample 3, some tiny pores were found at the interfaces, which indicated that the B_4C particles in a weak bonding layer with matrix would act as crack initiation sites, leading to the decrease in tensile strength. The addition of KBF_4 weakened the interface to some content, but induced the presence of more small-sized TiB_2 in the matrix and more homogeneous microstructure of composites. As a result, the tensile strength of composites firstly decreased and then increased as the addition of KBF_4 was increased.

4 Discussion

Based on the above results of microstructural evolution and mechanical properties of composites, it is clear that the B addition could optimize the distribution of B_4C and TiB_2 particles in the matrix and further induce the improvement in both strength and ductility of composites. In order to study the effects of B addition on the microstructure and mechanical properties of B_4C_p/Al composites, the reaction mechanism of Al(liquid)−B_4C−K_2TiF_6−KBF_4 system in ultrasonic field should be clarified.

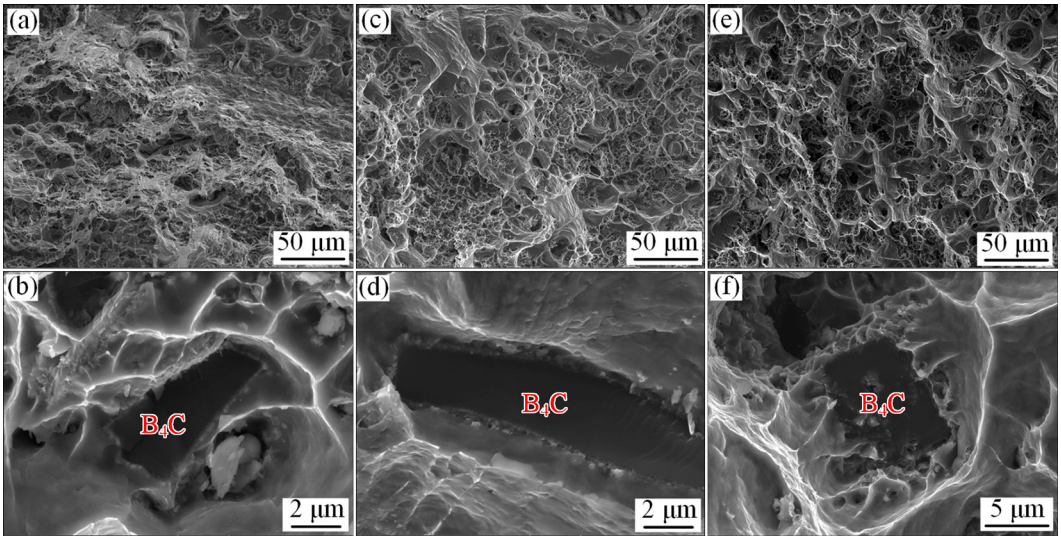

Fig. 8 Morphologies showing tensile fracture surfaces of three samples: (a, b) Sample 1; (c, d) Sample 2; (e, f) Sample 3

4.1 Reaction mechanism of Al−B_4C−K_2TiF_6−KBF_4 system

According to Refs. [14−16] which reported the reaction mechanism of Al(liquid)−B_4C−Ti system as well as the above experimental results, the potential reactions in the Al(liquid)−B_4C−K_2TiF_6−KBF_4 system can be deduced below.

When B_4C particles contact with liquid Al, Al_3BC and free [B] can be formed according to the reaction below:

$$B_4C+3Al(l)=Al_3BC+3[B] \quad (1)$$

As K_2TiF_6 and KBF_4 are added in the liquid Al, the [Ti] and [B] can be released from the two salts via the following reactions:

$$3K_2TiF_6+4Al(l)=3[Ti]+3KAlF_4+K_3AlF_6 \quad (2)$$

$$KBF_4+Al(l)=[B]+KAlF_4 \quad (3)$$

Accordingly, an Al(liquid)−[Ti]−[B] system can be obtained, in which the possible reactions are presented below:

$$3Al(l)+[Ti]=Al_3Ti \quad (4)$$

$$Al(l)+2[B]=AlB_2 \quad (5)$$

$$[Ti]+2[B]=TiB_2 \quad (6)$$

Among the three reaction products, TiB_2 (−189.851 kJ/mol) has the lowest Gibbs free energy compared with Al_3Ti (−4.614 kJ/mol) and AlB_2 (−136.040 kJ/mol) at 800 °C [10]. Thereby, Reaction (6) can take place most easily form the view point of thermodynamics. In the Al(liquid)−B_4C−K_2TiF_6−KBF_4 system, it should be noted that the [B] can be provided from B_4C and KBF_4, respectively. Thereby, it is reasonable that the addition amount of KBF_4 can directly influence the reaction sequence and further affect the phase formation (TiB_2, AlB_2 and Al_3BC).

4.2 Effect of B addition on microstructure of B_4C_p/Al composites

The reaction process of Al−B_4C−K_2TiF_6−KBF_4 system with regard to the addition amount of KBF_4 can be illuminated via the schematic diagram in Fig. 9, in which a B_4C particle is regarded as a sphere. For the system without KBF_4 addition (as shown in Fig. 9(a)), B_4C particles can easily enter into molten Al since the Al_2O_3 layer formed on the liquid Al surface is dissolved by the reaction products produced in Reaction (2) which improves the wettability between B_4C and Al [17]. Once the B_4C particle is exposed to the liquid Al, an Al_3BC layer can be formed on the B_4C surface. In the meantime, free [B] which diffuses into the adjacent liquid Al through the growing Al_3BC layer can easily combine with [Ti] to form TiB_2 phase which mainly locates on the B_4C surface. Our previous research clearly proved that the usage of ultrasound was able to lead to the rapid formation of a compact and continuous TiB_2 layer [10]. Hence, the interfacial reaction layer in Al(liquid)−B_4C−K_2TiF_6 system irradiated with ultrasound is composed of an inside Al_3BC layer and an outside TiB_2 layer. Due to the existence of TiB_2 layer which acts as a protective layer, Reaction (1) can be effectively inhibited.

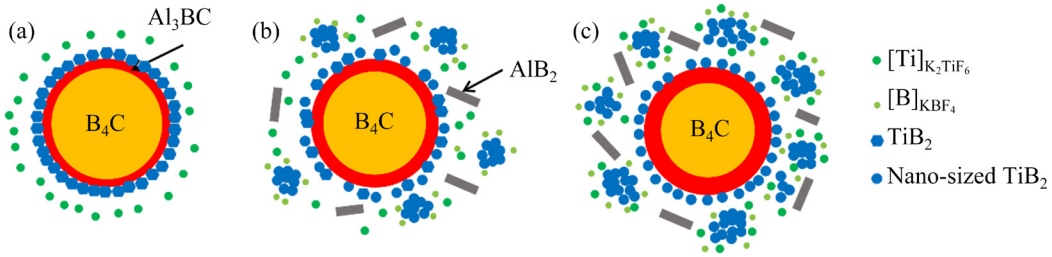

Fig. 9 Schematic diagrams of reaction mechanism with different contents of KBF_4: (a) K_2TiF_6; (b) KBF_4/K_2TiF_6 molar ratio of 1; (c) KBF_4/K_2TiF_6 molar ratio of 2

After a certain amount of KBF_4 (KBF_4/K_2TiF_6 molar ratio of 1) is introduced into the reaction system (as shown in Fig. 9(b)), [Ti] and [B] release from the molten salts via reduction reaction and diffuse into Al melt across the salts/Al interface. The concentrations of [Ti] and [B] reach the saturability rapidly in molten Al since the application of ultrasound [18], on the one hand, can facilitate the dissolution rate of [Ti] and [B] from the K_2TiF_6 and KBF_4; on the other hand, can make [Ti] and [B] have an opportunity to contact and reach saturability rapidly in molten Al. Then, around 50% of [Ti] combines with [B] to form small-sized TiB_2 particles in the matrix via a precipitation-growth mechanism. Finally, the residual [Ti] combines with [B] from B_4C to generate TiB_2 on B_4C surface, thereby both the thickness and continuity of TiB_2 layer on B_4C surface are decreased. Accordingly, the protective effect of TiB_2 layer is reduced, leading to the formation of AlB_2.

With the further increase of KBF_4 (KBF_4/K_2TiF_6 molar ratio of 2, as shown in Fig. 9(c)), nearly all the [Ti] is consumed by KBF_4 to form small-sized TiB_2 particles in the matrix. Thereby, B_4C particles are located in a [Ti]-poor environment and the formation of protective TiB_2 layer on the B_4C surface is rather limited, leading to the decomposition of B_4C and the generation of Al_3BC and AlB_2 in the matrix.

An interesting finding in this research is that adding B in the Al−B_4C−K_2TiF_6 system can significantly make the B_4C particles distribute more uniformly in the matrix using UAC method. According to MIRIHANAGE et al [19], the presence of nano particles in molten Al alloy, on the one hand, can enhance the ultrasonic cavitation effect since the nano particles can act as heterogeneous nuclei for cavitation bubble formation, on the other hand, can increase the melt streaming which results from the improved cavitation bubble activity. In this research, the addition of B can lead to the introduction of more small-sized TiB_2 particles into the matrix in the ultrasonic fields, and these small-sized TiB_2 particles can significantly intensify the ultrasonic stirring effect, which can break up the B_4C particle clusters and make the B_4C particles disperse in the matrix more homogeneously.

4.3 Effect of B addition on mechanical properties of composites

The above results clearly showed that the addition of B was beneficial to improving both the hardness and mechanical properties of the composites. After KBF_4 addition, more small-sized TiB_2 particles were formed and dispersed in the matrix rather than on the B_4C surface, which could increase the hardness of composites. It is well known that the reinforced particle with nano size (below 100 nm) has Orowan strengthening effect [20,21]. Thereby, more small-sized TiB_2 particles can lead to higher strength of composites. Besides, coefficient of thermal expansion (CTE) mismatch strengthening effect induced by the TiB_2 particles can also lead to the improvement in strengthening of composites [22,23]. However, it should be noted that the formation of TiB_2 layer on B_4C surface was inhibited, which reduced the strength of the composites to some extent since the TiB_2 layer was estimated to have a positive effect on the mechanical properties of the composites [11,24]. This is proposed to be the reason why the strength of Sample 2 decreased slightly compared to Sample 1. Since a large number of small-sized TiB_2 particles were generated in the matrix in Sample 3, the matrix can be further strengthened even though the B_4C_p/Al

interface may become weak. Hence, the YS and UTS of the samples firstly decreased and then increased with increasing [B] content. In addition, better spatial distribution of B_4C particles was conducive to the enhancement of El as well as the stability of composites.

5 Conclusions

(1) The thickness of TiB_2 layer on B_4C surface was decreased and more small-sized TiB_2 particles were induced into the matrix with increasing B content. The distribution of B_4C particles was also improved with the addition of KBF_4.

(2) The addition of KBF_4 could influence the reaction sequence and the phase formation of the composites, hence more small-sized TiB_2 particles were distributed in the matrix, which led to the intensification of cavitation as well as flow velocity and finally led to the homogeneous distribution of B_4C particles.

(3) The hardness and the mechanical properties of composites were both improved with the addition of KBF_4 due to the presence of TiB_2 particles in the matrix, and the stability of the composites was improved significantly due to the B addition induced homogeneous microstructure.

Acknowledgments

We would like to thank the National Natural Science Foundation of China (Nos. 52174372, 51974224), the Natural Science Foundation of Shaanxi Province, China (No. 2020JM-047), and the Fundamental Research Funds for Central Universities, China (No. xtr0118008) for their support. We also thank the Xi'an Jiaotong University Instrument Analysis Center for the help of the SEM analysis.

References

[1] TAN Xiao-fen, ZENG Fan-hao, WANG Shu-qiu, ZHOU Fei, XIONG Xiang. Effects of heat treatment on phase contents and mechanical properties of infiltrated B_4C/2024Al composites [J]. Transactions of Nonferrous Metals Society of China, 2014, 24: 2359−2365.

[2] LI Yu, LI Qiu-lin, LI Dong, LIU Wei, SHU Guo-gang. Fabrication and characterization of stir casting AA6061-31% B_4C composite [J]. Transactions of Nonferrous Metals Society of China, 2016, 26: 2304−2312.

[3] GUPTA R, NANDA T, PANDEY O P. Comparison of wear behaviour of LM13 Al−Si alloy based composites reinforced with synthetic (B_4C) and natural (ilmenite) ceramic particles [J]. Transactions of Nonferrous Metals Society of China, 2021, 31: 3613−3625.

[4] KENNEDY A R, BRAMPTON B. The reactive wetting and incorporation of B_4C particles into molten aluminium [J]. Scripta Materialia, 2001, 44: 1077−1082.

[5] BARADESWARAN A, PERUMAL A E. Influence of B_4C on the tribological and mechanical properties of Al 7075−B_4C composites [J]. Composites (Part B): Engineering, 2013, 54: 146−152.

[6] CHEN Mi, LIU Zhi-wei. Ultrasound assisted casting method for fabricating B_4C_p/Al composites with the addition of K_2ZrF_6 [J]. Materials Letters, 2020, 280: 128545.

[7] KAI Xi-zhou, WU Lin, PENG Yan-jie, TAN Zhan-qiu, LI Gui-rong, CHEN Gang, XU Xiao-jing, LI Zhi-qiang, ZHAO Yu-tao. Effects of Zr element on the microstructure and mechanical properties of B_4C/Al composites fabricated by melt stirring method [J]. Composites (Part B): Engineering, 2021, 224: 109156.

[8] NAMPOOTHIRI J, HARINI R S, NAYAK S K, RAJ B, RAVI K R. Post in-situ reaction ultrasonic treatment for generation of Al−4.4Cu/TiB_2 nanocomposite: A route to enhance the strength of metal matrix nanocomposites [J]. Journal of Alloys and Compounds, 2016, 683: 370−378.

[9] ESKIN G I. Broad prospects for commercial application of the ultrasonic (cavitation) melt treatment of light alloys [J]. Ultrasonics Sonochemistry, 2001, 8: 319−325.

[10] CHEN Mi, LIU Zhi-wei, ZHENG Qiao-ling, SUN Qing-qing, ZHENG Bo-han. Rapid preparation of B_4C_p/Al composites with homogeneous interface via ultrasound assisted casting method [J]. Journal of Alloys and Compounds, 2021, 858: 157659.

[11] LI Yu, LI Qiu-lin, LIU Wei, SHU Guo-gang. Effect of Ti content and stirring time on microstructure and mechanical behavior of Al−B_4C composites [J]. Journal of Alloys and Compounds, 2016, 684: 496−503.

[12] ZHANG Liu, SHI Guo-pu, KUN Xu, WU Hao, LI Qing-gang, WU Jun-yan, WANG Zhi. Phase transformation and mechanical properties of B_4C/Al composites [J]. Journal of Materials Research and Technology, 2020, 9: 2116−2126.

[13] LAI J, ZHANG Z, CHEN X G. Effect of Sc, Zr, and Ti on the interfacial reactions of the B_4C/Al system [J]. Journal of Materials Science, 2011, 46: 451−459.

[14] ZHANG J J, LEE J M, CHO Y H, KIM S H, YU Hua-shun. Effect of the Ti/B_4C mole ratio on the reaction products and reaction mechanism in an Al−Ti−B_4C powder mixture [J]. Materials Chemistry and Physics, 2014, 147: 925−933.

[15] ZHENG Ji-yun, LI Qiu-lin, LIU Wei, SHU Guo-gang. Microstructure evolution of 15 wt.% boron carbide/aluminum composites during liquid-stirring process [J]. Journal of Composite Materials, 2016, 50: 3843−3852.

[16] LIU Yu-xuan, WANG Ri-chu, PENG Chao-qun, CAI Zhi-yong, ZHOU Zhao-hui, LI Xiao-geng, CAO Xuan-yang. Microstructures and mechanical properties of in-situ TiB_2/Al−xSi−0.3Mg composites [J]. Transactions of Nonferrous Metals Society of China, 2021, 31: 331−344.

[17] NABAWY A M, CHEN X G. Fabrication of Al−TiB_2 nanocomposites by flux-assisted melt stirring [J]. Metallurgical and Materials Transactions B, 2015, 46:

1596−1602.

[18] LIU Z W, RAKITA M, XU W W, WANG X M, HAN Q Y. Ultrasound assisted salts–metal reaction for synthesizing TiB_2 particles at low temperature [J]. Chemical Engineering Journal, 2015, 263: 317−324.

[19] MIRIHANAGE W, XU W W, TAMAYO A J, ESKIN D, GRACIA F M, SRIRANGAM P, LEE P. Synchrotron radiographic studies of ultrasonic melt processing of metal matrix nano composites [J]. Materials Letters, 2016, 164: 484−487.

[20] ZHANG Z, CHEN D L. Consideration of Orowan strengthening effect in particulate-reinforced metal matrix nanocomposites: A model for predicting their yield strength [J]. Scripta Materialia, 2006, 54: 1321−1326.

[21] XIAO Hong-yu, LI Yu-gang, GENG Ji-wei, LI Hong-ping, WANG Ming-liang, CHEN Dong, LI Zhu-guo, WANG Hao-wei. Effects of nano-sized TiB_2 particles and Al_3Zr dispersoids on microstructure and mechanical properties of Al−Zn−Mg−Cu based materials [J]. Transactions of Nonferrous Metals Society of China, 2021, 31: 2189−2207.

[22] ZHAO Bo-wen, YANG Qing, WU Liang, LI Xian-feng, WANG Ming-liang, WANG Hao-wei. Effects of nanosized particles on microstructure and mechanical properties of an aged in-situ TiB_2/Al−Cu−Li composite [J]. Materials Science and Engineering A, 2019, 742: 573−583.

[23] FAN Cai-he, OU Ling, HU Ze-yi, YANG Jian-jun, CHEN Gang, YAN Hong-ge. Microstructures and mechanical properties of BP/7A04 Al matrix composites [J]. Transactions of Nonferrous Metals Society of China, 2019, 29: 2027−2034.

[24] HU Qi-yao, ZHAO Hai-dong, GE Ji-long. Microstructure and mechanical properties of (B_4C+Al_3Ti)/Al hybrid composites fabricated by a two-step stir casting process [J]. Materials Science and Engineering A, 2016, 650: 478−482.

B 元素添加对超声辅助铸造法制备 B_4C_p/Al 复合材料显微组织和力学性能的影响

陈 咪[1]，刘志伟[1]，贾豫冬[2]，余申卫[3]，何 源[3]，郑博瀚[2]

1. 西安交通大学 材料科学与工程学院 金属材料强度国家重点实验室，西安 710049；
2. 西北有色金属研究院，西安 710016；
3. 中国船舶集团有限公司 第十二研究所，兴平 713102

摘 要：通过在 Al−B_4C−K_2TiF_6 反应体系中添加 KBF_4 引入 B 元素，采用超声辅助铸造法制备 B_4C_p/Al 复合材料。研究 B 元素添加对复合材料显微组织、力学性能及界面反应机理的影响。实验结果表明，添加 B 元素可以改变 B_4C_p/Al 的界面结构，使更多的小粒径 TiB_2 颗粒分布在基体中，因此空化和声流效应进一步增强，熔体中的 B_4C 团簇被破碎，使复合材料组织更加均匀、综合力学性能得到改善。

关键词：B 元素；B_4C_p/Al 复合材料；显微组织；力学性能；界面反应；超声波；铸造法

(Edited by Wei-ping CHEN)